Morphology and Scaling of Impact Craters in Granular Media

Amanda M. Walsh,[1] Kristi E. Holloway,[1] Piotr Habdas,[2] and John R. de Bruyn[1]

[1]*Department of Physics and Physical Oceanography, Memorial University of Newfoundland, St. John's, Newfoundland, Canada A1B 3X7*

[2]*Department of Physics, Emory University, Atlanta, Georgia 30322-2430, USA*

(Received 17 February 2003; revised manuscript received 27 June 2003; published 4 September 2003)

We present the results of experiments on impact craters formed by dropping a steel ball vertically into a container of small glass beads. As the energy of impact increases, we observe a progression of crater morphologies analogous to that seen in craters on the moon. We find that both the diameter and the depth of the craters are proportional to the 1/4 power of the energy. The ratio of crater diameter to rim-to-floor depth is constant for low-energy impacts, but increases at higher energy, similar to what is observed for lunar craters.

DOI: 10.1103/PhysRevLett.91.104301 PACS numbers: 45.70.–n, 83.80.Fg, 96.35.Gt

Craters on the moon and planets have been of scientific interest since they were first observed. Their origin in impact events was suggested (and rejected) by Hooke in 1665 [1], and not fully accepted until early in the 20th century [2,3]. The formation of impact craters is an extremely complex process, depending on the material properties of both target and projectile, the parameters of the impact, as well as on gravity and atmospheric effects. Their morphology depends largely on impact energy [2,4], with features such as central peaks, slump terraces, and multiple rings appearing as the size of the crater increases. The scaling of crater dimensions has been studied [5], and power-law relationships between crater diameter w and the energy of impact E can be derived in certain limits. In the gravity-dominated limit, the kinetic energy of the projectile goes into lifting material out of the crater against gravity and depositing it on the surface [2,5]. The energy required to excavate the crater is then proportional to its volume times its depth. Assuming that the crater's depth is proportional to w, this energy is proportional to w^4, so we expect $w \propto E^{1/4}$. On the other hand, if the process is dominated by the strength of the target material, one finds $w \propto E^{1/3}$ [2,5]. There have been many laboratory studies of impact crater formation [3,6,7], but most have involved hypervelocity projectiles fired into a target with speeds on the order of a kilometer per second [8]. Quite recently, experiments on low-energy impacts in granular materials have been reported [7]; that work focused on the depth of penetration of the projectile and the nature of the force exerted on it by the granular medium [9].

In this Letter we report on experiments on impact craters formed by dropping a ball into a container of fine granular material. We study the morphology of the craters produced and the scaling of crater dimensions with energy. Despite the very large difference in energy scales, we observe both qualitative and quantitative similarities with lunar and planetary craters.

Our experiments were performed by releasing a 2.54 cm diameter steel ball of mass 66.0 g from a holder so that it fell vertically into a container of loosely packed small glass beads. Five different bead sizes were used, ranging from 45–90 μm up to 300–425 μm. Compaction of the target material has a large effect on crater formation: with the smallest beads, lightly shaking the container even once dramatically reduced the penetration of the steel ball. To control this, the beads were poured evenly into the experimental container prior to each run. The two smallest sized beads were poured through a sieve. Apart from smoothing of the surface with a straight edge, they were used "as poured" without any shaking.

The impact energy E is just the kinetic energy of the ball, and is proportional to the release height h. We varied h from 2 to 90 cm, corresponding to impact velocities u of order 10^2 cm/s and impact energies from 10^5 to 6×10^6 ergs. In most cases, the steel ball was completely buried in the target material after the impact, but for low energies and larger beads, a portion of the ball remained exposed. The impacts are characterized by the inverse Froude number, $\mathrm{Fr}^{-1} = gD_b/2u^2$, the ratio of gravitational to dynamic pressures. Here g is the acceleration due to gravity and D_b is the diameter of the ball. In our work $0.007 < \mathrm{Fr}^{-1} < 0.32$, while for planetary impact craters $10^{-6} \lesssim \mathrm{Fr}^{-1} \lesssim 10^{-2}$ [5]. Our experiments overlap with the high end of this range. In contrast, hypervelocity impact experiments are typically limited to $\mathrm{Fr}^{-1} \lesssim 10^{-6}$ [5].

Figure 1 shows examples of the crater morphologies observed. At low energies and with large beads, simple craters as in Fig. 1(a) are formed. These are bowl-shaped and surrounded by a uniform rim raised above the original surface level of the beads. As E increases or the bead size D_g decreases, a peak appears in the center of the crater, as in Fig. 1(b), associated with the appearance of granular jets [10–12]. As the ball enters the target, beads are pushed outwards. These beads then collapse back inwards, collide with each other, and are forced upwards into a jet. For a given D_g, the height of the jet is approximately proportional to E [10,11]. In the case of Fig. 1(b)

 © 2003 The American Physical Society

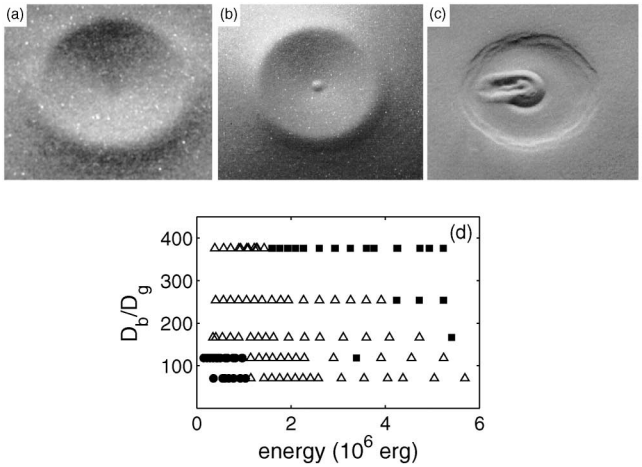

FIG. 1. Impact craters formed by dropping a 2.54 cm diameter, 66.0 g steel ball vertically into a container of small glass beads. (a) A simple crater formed in beads of diameter $D_g = 180$–$250\ \mu$m when the ball was released from a height h of 14.8 cm. The rim-to-rim crater diameter w is 6.62 cm. (b) A crater with a small central peak and $w = 8.08$ cm. Here $h = 32.5$ cm and $D_g = 180$–$250\ \mu$m. (c) A complex crater with $w = 5.66$ cm formed in beads with $D_g = 45$–$90\ \mu$m for $h = 40.1$ cm. (d) The range of existence of the different crater morphologies in terms of the impact energy and the ratio of the ball diameter to the bead diameter, D_b/D_g. Circles: simple craters; triangles: craters with a central peak; squares: craters with multiple rings.

the jet was small and a modest peak is formed. Figure 1(c) shows a crater formed at higher energy with the smallest beads. The crater rim is less well defined and the walls of the transient original crater were steep enough to be gravitationally unstable and so have collapsed, resulting in slump terraces around the crater's perimeter. The complex central structure results from the collapse of a much larger jet [13]. At the highest energies studied, in addition to the features seen in Fig. 1(c), one or more large, low rings form well outside the main crater rim, and the details of the morphology within the main crater become quite complex [10]. Figure 1(d) shows the range of E and D_g over which the different morphologies are observed. Transitions between morphologies depend on both these parameters.

The same sequence of crater morphologies is observed in craters on the moon and elsewhere [2,4]. Lunar craters up to about 15 km in diameter are simple bowl-shaped craters. Larger craters have central peaks or peak rings; an inertial focusing mechanism similar to that described above is believed to play an essential role in their formation. Slump terraces around the rim of complex craters result from gravitational collapse of steep transient crater walls. The largest impact features on the moon and planets are multi-ringed basins hundreds of kilometers in diameter. Their formation is not well understood, but our results suggest that the process is simply a higher-energy variant of that which forms smaller craters, and not anything fundamentally different.

The inset of Fig. 2 is a log-log plot of the crater diameter w, measured at the top of the crater rim, as a function of h. The colors indicate different bead sizes, while the symbols show the crater morphology. There is no effect of particle size for the four larger bead sizes. The data for these beads all fall on the same line, and a fit to all four data sets simultaneously gives a slope of 0.251 ± 0.005. This $1/4$ power law is in agreement with previous results [6,7] and with the above prediction for the gravity-dominated regime [2,5]. The smallest (45–90 μm) beads behave differently and will be discussed below. To express our data in dimensionless form, we scale distances by D_g and energies by E_0, the energy required to raise one bead a distance D_g against gravity; $E_0 = \frac{1}{6}\pi D_g^4 \rho_g g$. Thus the scaled crater diameter $w' = w/D_g$, while the scaled impact energy is

$$E' = E/E_0 = \frac{h}{D_g}\frac{\rho_b}{\rho_g}\left(\frac{D_b}{D_g}\right)^3, \qquad (1)$$

where ρ_g and ρ_b are the densities of the beads and ball, respectively. The same scaling was obtained from a combination of dimensional arguments and experiments in Ref. [7]. w' is plotted against E' in Fig. 2. Except for a few points at the very highest E', the data for the four larger D_gs are well described by a $1/4$ power law over more than

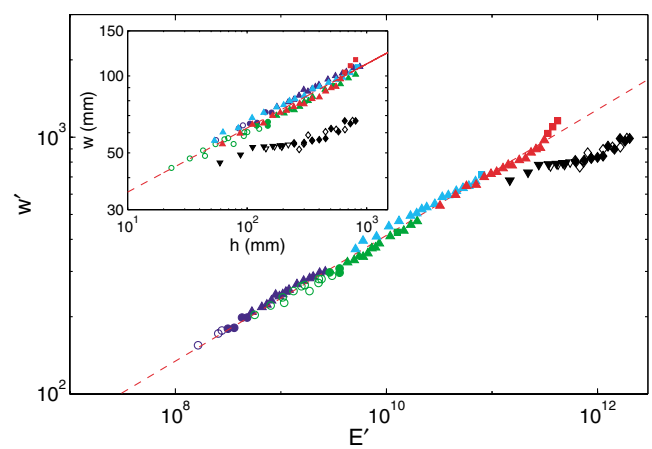

FIG. 2 (color). The inset shows crater diameter w vs release height h. Dark blue symbols: $D_g = 300$–$425\ \mu$m; green symbols: 180–250 μm; light blue symbols: 125–180 μm; red symbols: 75–125 μm; and black symbols: 45–90 μm. Circles indicate simple craters; upward-pointing triangles, craters with a central peak; squares, multi-ring craters; downward-pointing triangles, craters with slump terraces around the rim; and diamonds, multi-ring craters with slump terraces. Open circles indicate runs for which the steel ball did not completely penetrate into the target material. The dashed line is a fit to the data for the four larger bead sizes and has a slope of 0.251 ± 0.005. The main graph shows the same data scaled as described in the text. The dashed line is again a fit for the four larger bead sizes; its slope is 0.245 ± 0.002.

3 orders of magnitude in E'. The deviations at high E' correspond to multi-ring craters, which suggests a change in the energetics of the crater formation process associated with the change in morphology.

The diameters of craters in the smallest beads (black symbols) fall significantly below the other data. Two sets of data with these beads taken several months apart are plotted as open and solid black symbols in Fig. 2; they are indistinguishable. In this case w increases very slowly, particularly at low E. There are several reasons for this different behavior. First, although granular jets appear for all conditions under which complex craters are formed [see Fig. 1(d)], they are relatively small for all but the 45–90 μm beads. For these beads, however, the jets are quite spectacular—the jet height j can be larger than h, and a significant fraction of the impact energy goes into their generation [10]. This implies a smaller w for a given E for these beads, as observed. Assuming that the impact energy is used to raise material excavated from the crater a height proportional to j, an argument similar to that used to derive the 1/4 scaling law gives $E \propto w^3 j$. Taking $j \propto E$ [10,11] gives $w =$ const. The observed slow variation of w with E is consistent with this prediction. Other factors affecting these beads are air drag, which strongly affects the flow of these small particles after impact, and cohesion, which likely arises due to atmospheric humidity—a thin surface film of water on the beads leads to the formation of liquid bridges when they come in contact [14].

The formation of terraces around the crater rim as in Fig. 1(c) requires the granular medium to have some material strength. Terracing was observed only for the smallest beads, indicating the importance of cohesive forces for these particles. By calculating the pressure required to overcome the shear strength of the rock, the width s of the first slump terrace in gravitationally unstable lunar craters has been related to the cohesive strength c of the material [15]. The result is

$$s = \frac{c}{\rho g}\left(\frac{1 + 16\lambda^2}{16\lambda^2}\right), \tag{2}$$

where λ is the depth-to-diameter ratio of the initial transient crater and ρ is the density of the target material. From our measurements we find $\lambda \approx 1/8$ (see below). Assuming the beads are random loose packed and using a typical terrace width of 0.22 cm for our craters, we find $c = 57$ dyn/cm^2. This is consistent in magnitude with liquid bridges being the source of the cohesion.

Figure 3 shows the scaled crater depth d', measured from the original surface level to the lowest point in the crater, as a function of E'. In runs for which the ball remained partly exposed, the lowest point is where it emerges from the beads. When the ball is completely buried, d is measured to the center of the crater (for simple craters) or the base of the central peak (for complex craters). Neglecting runs for which the ball was not completely buried, the individual data sets are each well described by a 1/4 power law in E', as indicated for the largest beads by the dashed line in Fig. 3. The average exponent obtained from similar fits to all five data sets is 0.26 ± 0.05. However, while the power-law *exponent* does not depend on D_g within our uncertainties, our scaling does not completely account for the effects of particle size here, and the data do not collapse onto a single line [16]. As Fig. 3 indicates, craters in smaller beads are shallower than an extrapolation of a fit to the largest beads would predict, likely due to the increased effects of air drag and cohesion for the smaller beads. At low E', when the steel ball is not completely buried, the dependence of d' on energy is steeper [9].

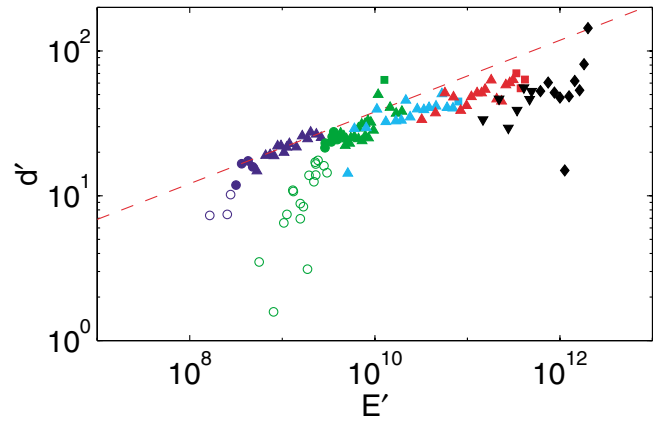

FIG. 3 (color). A plot of the scaled crater depth as a function of scaled energy. The symbols are as in Fig. 2. The dashed line is a fit to the data for the 300–425 μm beads (dark blue symbols), excluding those for which the steel ball did not completely penetrate the beads. It gives a slope of 0.248 ± 0.011.

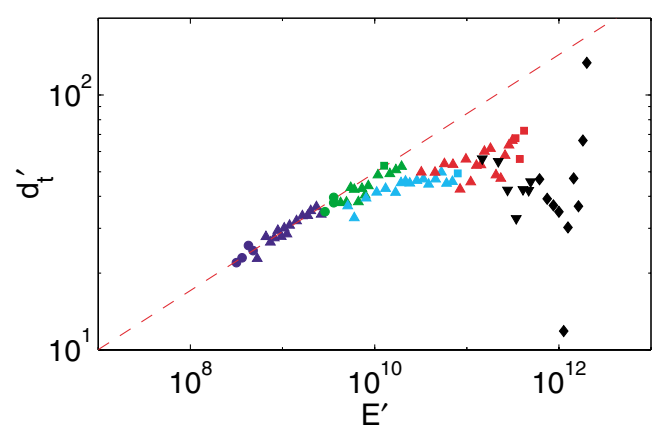

FIG. 4 (color). A plot of the scaled rim-to-floor depth as a function of scaled energy. The symbols are as in Fig. 2. The dashed line is a fit to the data for $D_g = 300$–425 μm (dark blue symbols), and has a slope of 0.231 ± 0.016. Points for which the ball was not completely buried are not shown and were excluded from the fit.

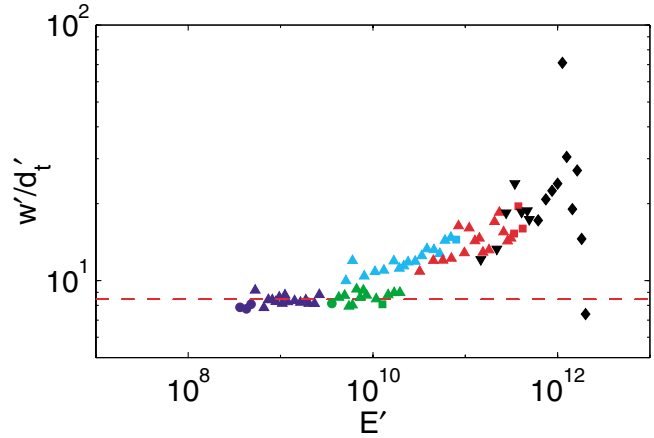

FIG. 5 (color). A plot of the ratio of crater diameter to rim-to-floor depth as a function of scaled energy. The symbols are as in Fig. 2. The dashed line indicates the mean of the ratio for the largest beads (dark blue symbols).

We also measured the depth d_t from the top of the crater rim to the lowest point on the crater floor. This quantity differs from d in two ways. First, there is the obvious addition of the height of the rim above the surface. Second, especially for the smaller beads the target was significantly compacted by the impact, so that the local surface level was lower after the impact than before. For the smallest beads, this resulted in d_t actually being *smaller* than d. These data (scaled as above) are shown in Fig. 4. The rim-to-floor depth is well described by a power law with an exponent close to $1/4$ at low E' but flattens out at higher energies, suggesting a change in the details of the crater formation process at high E'.

The ratio of crater diameter to rim-to-floor depth has been measured for lunar craters; it is approximately 5 for simple craters (i.e., low energies) but becomes larger for complex craters (high energies) [2]. Figure 5 shows this ratio from our data; it is constant with a mean value of 8.4 ± 0.4 for $E' \lesssim 10^{10}$, but increases at higher energies. The low-energy value is slightly higher than for lunar craters, probably due to differences in material properties, but the same trend is observed as E' is increased — craters formed in high energy impacts are relatively wider and flatter than low-energy craters.

The energy of the impact that formed the 1 km diameter Meteor Crater in Arizona is estimated to be on the order of 10^{22} erg [2]. In contrast, the impacts studied here have energies of order 10^6 erg. Despite the 16-order of magnitude difference in energy scales, we observe trends in both the morphology and the scaling of crater size with energy that are remarkably similar to those seen in lunar craters, and which can be explained with the same physics. While the details of the physical processes involved are, of course, very different, our results nonetheless suggest that many of the important aspects of large-scale crater formation, such as fluidization and morphology selection, can be meaningfully modeled in low-energy laboratory experiments on granular media.

This research was supported by NSERC of Canada. We are grateful to D. Durian, J. Melosh, and G. Collins for helpful discussions.

[1] R. Hooke, *Micrographia* (Dover, New York, 1961).
[2] H. J. Melosh, *Impact Cratering: A Geologic Process* (Oxford University Press, New York, 1989).
[3] A. Wegner, The Moon **14**, 211 (1975), translated by A. M. Celâl Şengör.
[4] H. J. Melosh and B. A. Ivanov, Annu. Rev. Earth Planet. Sci. **27**, 385 (1999).
[5] K. A. Holsapple, Annu. Rev. Earth Planet. Sci. **21**, 333 (1993).
[6] J. C. Amato and R. E. Williams, Am. J. Phys. **66**, 141 (1998).
[7] J. S. Uehara, M. A. Ambroso, R. P. Ojha, and D. J. Durian, Phys. Rev. Lett. **90**, 194301 (2003).
[8] P. H. Schultz, Int. J. Impact Engng. **5**, 569 (1987).
[9] In [7] the impacting ball never completely penetrated the target material, while in our experiments it did, except at very low E for large beads. The depth defined in [7] is the penetration depth of the impacting ball, measured from the original surface to the bottom of the ball. In contrast, we measure the crater depth from the original surface to the bottom of the crater. These quantities are not simply related, so the $1/3$ power law for the penetration depth reported in [7] cannot be compared with the results presented here. In additional work to be reported elsewhere [10], we find a $1/3$ power law for the penetration depth with our larger beads, but a $1/2$ power law with smaller beads.
[10] A. Walsh and J. R. de Bruyn (unpublished).
[11] S. T. Thoroddsen and A. Q. Shen, Phys. Fluids **13**, 4 (2001).
[12] R. Mikkelsen, M. Versluis, E. Koene, G.-W. Bruggert, D. van der Meer, K. van der Weele, and D. Lohse, Phys. Fluids **14**, S14 (2002).
[13] We note the intriguing similarity in appearance between the central structure of the crater in Fig. 1(c) and that of the King crater on the moon. See, for example, Fig. 2.10 of Ref. [2].
[14] R. Albert, I. Albert, D. Hornbaker, P. Schiffer, and A. L. Barabási, Phys. Rev. E **56**, R6271 (1997); P. Tegzes, R. Albert, M. Paskvan, A.-L. Barabási, T. Vicsek, and P. Schiffer, Phys. Rev. E **60**, 5823 (1999); T. C. Halsey and A. J. Levine, Phys. Rev. Lett. **80**, 3141 (1998).
[15] H. J. Melosh, in *Impact and Explosion Cratering*, edited by D. J. Roddy, R. O. Pepin, and R. B. Merrill (Pergamon, New York, 1977), p. 1245; S. J. Pearce and H. J. Melosh, Geophys. Res. Lett. **13**, 1419 (1986).
[16] A power-law fit to all five data sets simultaneously gives an exponent too low to be consistent with the fits to the individual sets.